A rotational and vibrational investigation of phenylpropiolonitrile (C₆H₅C₃N)

Zachary Buchanan [a,b,*], Kin Long Kelvin Lee [c], Olivia Chitarra [a], Michael C. McCarthy [c], Olivier Pirali [a,d], Marie-Aline Martin-Drumel [a]

[a] *Université Paris-Saclay, CNRS, Institut des Sciences Moléculaires d'Orsay, 91405 Orsay, France*
[b] *Department of Chemistry, The University of California Davis, Davis, CA, USA*
[c] *Center for Astrophysics | Harvard & Smithsonian, Cambridge, MA 02138, USA*
[d] *SOLEIL Synchrotron, AILES beamline, l'Orme des Merisiers, Saint-Aubin, 91190 Gif-sur-Yvette, France*

ABSTRACT

The evidence for benzonitrile (C_6H_5CN) in the starless cloud core TMC–1 makes high-resolution studies of other aromatic nitriles and their ring-chain derivatives especially timely. One such species is phenylpropiolonitrile (3-phenyl-2-propynenitrile, $C_6H_5C_3N$), whose spectroscopic characterization is reported here for the first time. The low resolution (0.5 cm^{-1}) vibrational spectrum of $C_6H_5C_3N$ has been recorded at far- and mid-infrared wavelengths (50–3500 cm^{-1}) using a Fourier Transform interferometer, allowing for the assignment of band centers of 14 fundamental vibrational bands. The pure rotational spectrum of the species has been investigated using a chirped-pulse Fourier transform microwave (FTMW) spectrometer (6– 18 GHz), a cavity enhanced FTMW instrument (6–20 GHz), and a millimeter-wave one (75–100 GHz, 141–214 GHz). Through the assignment of more than 6200 lines, accurate ground state spectroscopic constants (rotational, centrifugal distortion up to octics, and nuclear quadrupole hyperfine constants) have been derived from our measurements, with a plausible prediction of the weaker lines through calculations. Interstellar searches for this highly polar species can now be undertaken with confidence since the astronomically most interesting radio lines have either been measured or can be calculated to very high accuracy below 300 GHz.

© 2021 Published by Elsevier Inc.

1. Introduction

The ubiquity of aromatic molecules is closely-correlated to their stability and lack of reactivity, with functionalized aromatics serving as a common motif in biological chemistry. Polycyclic aromatic hydrocarbons are a prominent class of aromatics; they are well-known constituents in the outflows of certain evolved carbon stars and common byproducts in incomplete combustion processes [1–3]. From a purely spectroscopic viewpoint, a number of simple derivatives of benzene —the prototypical aromatic ring C_6H_6— have either not been characterized at all or at insufficient resolution to undertake an astronomical search in the coldest most quiescent molecular clouds in space. The recent discovery of benzonitrile —the simplest aromatic nitrile (C_6H_5CN or PhCN hereafter)— using radio observations towards Taurus Molecular Cloud (TMC-1) [4] has reignited the interest in nitrogen-containing aromatics generally and CN-functionalized aromatics specifically [5].

The subsequent identification of cyanocyclopentadiene, C_5H_5CN, in the same cloud [6] has only intensified this interest. Nitriles are also known to be important constituents in the chemistry of Titan's atmosphere [7], and they are very prominent in the interstellar medium (ISM), accounting for roughly 20% of the 220 or so molecules detected in the ISM to date, including cyanopolyynes as long as $HC_{11}N$ [8].

The presence of a nitrile group often imparts a molecule with a large permanent dipole moment and an intense rotational spectrum. In the case of PhCN, replacing a single H atom in benzene with a CN group transforms an otherwise highly symmetric ring into a highly polar species ($\mu_a = 4.5$ D; [9]) thereby greatly aiding its detection both in the laboratory and in space. Whilst the rotational spectrum of PhCN has been known for more than half-a-century [10], its interstellar detection was greatly aided by measurements at very high accuracy (*i.e.*, at a resolving power $f/\Delta f > 10^6$) at centimeter wavelengths [4,9]. In light of this finding, new —or in many cases improved— high-resolution studies of molecules closely related in structure and composition are worth pursuing.

---

* Corresponding author.
  E-mail address: zsbuchanan@ucdavis.edu (Z. Buchanan).

In this work, we report a combined pure rotational and vibrational investigation of a derivative of PhCN, phenylpropiolonitrile (3-phenyl-2-propynenitrile, $C_6H_5C_3N$, abbreviated as PhC_3N in the following) where the nitrile group is replaced by a longer chain variant (C_3N) (Fig. 1). This species has previously been identified as a possible product from the reaction between the cyano radical and phenylacetylene (C_6H_5CCH) [11]. To the best of our knowledge, however, spectroscopic investigations have been limited to experimental and theoretical vibronic spectroscopy [12,13] while high-resolution, rotationally-resolved studies are apparently lacking. In light of the large permanent electric dipole moment calculated here (5.9 D), laboratory measurement of rotational frequencies would allow astronomical searches for this ring-chain to be undertaken with little or no ambiguity. If found in space, the abundance of PhC_3N would provide a key test for models of aromatic chemistry which are poorly constrained at present. The infrared spectrum of PhC_3N is also of interest as a point of comparison with other benzene derivatives whose vibrational spectra are often plagued by a myriad of perturbations and resonances, notably Fermi and Darling-Dennison in the C—H and C≡C stretching regions [14–16], in addition to Fermi and Coriolis interactions for low frequency (~ 150 cm^{-1}), large amplitude modes that are prominent at room temperature [17–19]— even under astronomical conditions.

2. Experimental and computational methods

2.1. Quantum chemical calculations

Calculations were performed using the Gaussian'16 suite of electronic structure programs [20]. The goal of these calculations was to provide accurate estimates of spectroscopic parameters, including rotational constants, dipole moment, rotation-vibration corrections, and fundamental vibrational frequencies using second-order vibrational perturbation theory (VPT2). Geometry optimizations of PhC_3N and four of its isomers—namely the isocyanide analog PhCCNC and three variants where CN is substituted for a H atom on the ring of phenyl acetylene to yield *ortho-, meta-,* and *para*-cyanoethynylbenzene (CEB)—were carried out at the ωB97X-D/cc-pVQZ level on an ultrafine integration grid, in which optimized structures are those in which convergence to better than 10^{-5} of the root-mean-squared (RMS) value of the gradient has been achieved. For PhC_3N, we also performed (an)harmonic frequency analysis, obtaining both the harmonic and anharmonic vibrational frequencies and intensities at the same level of theory; with the latter, the rotation-vibration interaction constants α were computed. Cartesian coordinates of the optimized equilibrium structures can be found in Tables S1-S5 in the Supporting Information.

In addition to spectroscopic parameters, we have also performed rudimentary thermochemical calculations on the relative energies of PhC_3N and its isomers using the G3//B3LYP composite method [21], which has been shown to provide near-chemical accuracy at excellent computational cost [22]. Given that semi-empirical methods typically perform best on closed-shell molecules with relatively simpler electronic structure, as the ones studied here, we believe these calculations provide a quantitative determination of relative stabilities, accurate to ±4 kJ/mol.

2.2. Fourier-transform infrared measurements

The gas-phase vibrational spectrum of PhC_3N was recorded in the far-infrared (far-IR) and mid-infrared (mid-IR) using the Bruker IFS 125 Fourier transform (FT) interferometer located at the AILES beamline of the SOLEIL synchrotron facility (no synchrotron radiation was used in the present study) [23]. For the far-IR measurements, the spectrometer was equipped with a 6 μm mylar-silicon composite beamsplitter and a liquid helium-cooled silicon bolometer. A KBr beamsplitter and a sensitive HgCdTe detector, equipped with a cryogenically cooled entrance iris and optical filters [24], were used in the mid-IR region. Vapor of PhC_3N was injected in a White-type multipass cell aligned to yield a 150 m optical path length [25] and isolated from the interferometer by 50 μm-thick polypropylene windows in the far-IR and wedged ZnSe windows in the mid-IR range. In both spectral regions, the interferometer was continuously evacuated to 10^{-5} mbar to minimize absorption from residual water. Spectra were recorded at a resolution of 0.5 cm^{-1} using a globar light source and an entrance iris of 4 mm, and consist of 100 and 500 co-added interferograms for the far-IR and mid-IR regions, respectively. Both spectra were recorded at a sample pressure of 5 μbar. It is worth noting that the rotational structure within the vibrational bands could not be resolved even at the highest resolution of the spectrometer (0.001 cm^{-1}).

2.3. Chirped-pulse Fourier-transform microwave measurements

Microwave measurements were performed using a chirped-pulse Fourier transform microwave (CP-FTMW) spectrometer located at the Center for Astrophysics [26] which operates between 8 and 18 GHz. About 0.3 g of solid PhC_3N was introduced into a reservoir located behind the pulsed nozzle and Ne carrier gas (at a flow of ~20 sccm at standard temperature and pressure) passed through the reservoir; the resulting gas mixture was then injected into the vacuum chamber by operating the pulsed valve at a very low repetition rate (5 Hz). Because the vapor pressure of PhC_3N is relatively high at room temperature (several mbar), it was not necessary to heat the reservoir to observe rotational lines in the CP-FTMW spectrum with good signal-to-noise ratios.

Approximately 17,000 nozzle pulses, each probed by 10 microwave chirps, were acquired. Additional details on the experimental set-up are provided in Ref. [26]. The resulting spectrum, with electronics artifacts and well-known contaminant lines (*e.g.*, acetone) removed, is displayed in Fig. 2. Transitions with $5 \leqslant J'' \leqslant 15$ and $K_a'' \leqslant 4$ are visible.

2.4. Cavity-based Fourier-transform microwave measurements

In parallel to the present investigation, pure rotational transitions of PhC_3N were also identified by several of the co-authors of this paper while analyzing the discharge products of a benzene/nitrogen (N_2) mixture [28]. Using a cavity-enhanced FTMW
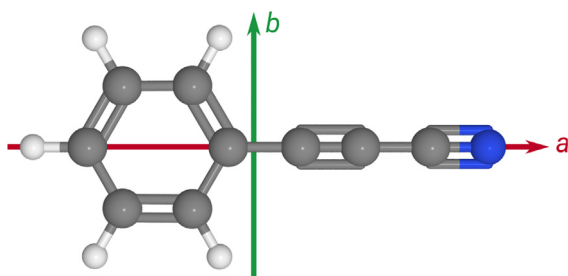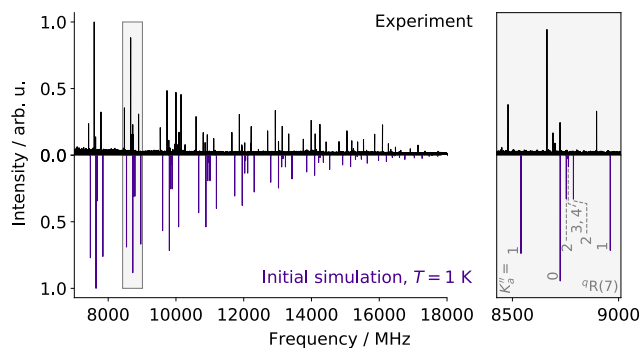

Fig. 1. Molecular structure of PhC$_3$N; *a* and *b* principal inertial axes are indicated (in red and green, respectively); the *c*-axis extends out of the molecular plane and is not shown.

Fig. 2. Experimental CP-FTMW spectrum (in black) of PhC_3N in comparison with a simulation at $T_{rot} = 1$ K (in purple) using the calculated set of rotational constants; the simulation is plotted here with negative intensity to more easily compare the two spectra. *Left panel:* the full spectrum, noting that a few lines originating from impurities are visible around 10 GHz; *Right panel:* expanded view around the ${}^qR(7)$ transitions, as indicated by the gray rectangle on the left panel. The simulation was performed using PGOPHER [27].

(CE-FTMW) spectrometer operating between 6 and 40 GHz, transitions of PhC_3N were measured at roughly ten times higher spectral resolution than can be achieved with the CP-FTMW instrument. In the following, we only briefly summarize the experimental conditions relevant to this work; further details about the CE-FTMW instrument and the discharge mixture experiments are presented in Refs. [26,28], respectively.

PhC_3N was synthesized by subjecting a mixture of C_6H_6 and N_2 diluted heavily in Ne to a high-voltage discharge (800 V); typical flow rates were 14, 12, and 20 sccm respectively. Compared to the CP-FTMW measurements where PhC_3N was the precursor, the discharge experiment results in a slightly higher rotational temperature, *i.e.*, ~ 10 K and produces rotational lines with demonstratively lower signal-to-noise ratio. Nevertheless, at the highest resolving power ($\sim 10^7$) the nitrogen nuclear-quadrupole structure for several low-K_a transitions ($K_a'' = 0 - 2$) in the 6–20 GHz region was partially resolved.

2.5. Absorption millimeter-wave measurements

The room temperature spectrum of PhC_3N was recorded at ISMO with an absorption spectrometer in which a frequency multiplication scheme is used to generate millimeter-wave radiation [29]. By combining the output of a radiofrequency synthesizer (Rohde & Schwarz) operating in the 2–20 GHz region with one of two amplifier / multiplier chains, it is possible to produce broadly tunable radiation with modest power (of a few mW) throughout the millimeter band; a Radiometer Physics GmbH (RPG) SMZ110 for 75–97 GHz measurements, and a Virginia Diodes Inc. (VDI) for those in the range 141–214 GHz.

The millimeter-wave radiation was collimated using a 10 mm focal length Teflon lens into a 2 m long Pyrex absorption cell and further focused onto a Schottky diode detector from VDI, using a second identical lens. The input radiation was frequency modulated at a frequency of 48.2 kHz and a commercial lock-in amplifier (Ametek) demodulated the signal at the second harmonic. The spectrum was recorded using 50 kHz frequency steps, a time constant of 50/100 ms, and an FM deviation of 200/250 kHz (where the two values refer the lower/higher frequency measurements, respectively).

A flow of PhC_3N, not exceeding a pressure of 2 μbar, was pumped through the cell and evacuated by a turbomolecular pump. Above this pressure, significant pressure broadening of the rotational lines was observed.

3. Results and discussion

3.1. Spectroscopic considerations

PhC_3N belongs to the C_{2v} symmetry group and possesses a $\tilde{X}^1A_1$ electronic ground state with 39 modes of vibration following the irreducible representation $\Gamma = 14A_1 \oplus 3A_2 \oplus 9B_1 \oplus 13B_2$. All vibrational modes except those of A_2 symmetry are IR active; A_1 and B_2 modes correspond to in-plane vibrations (respectively *a*- and *b*-type bands) while B_1 modes are out-of-plane vibrations (*c*-type bands). PhC_3N is a prolate asymmetric top molecule with a permanent dipole moment of 5.9 Debye along the *a* axis (axis of the C_3N bonds, Fig. 1), according to our calculations. PhC_3N also has nitrogen nuclear quadrupole hyperfine structure, but this splitting is only partially resolved at low frequency in the CE-FTMW measurements. Given that the molecule has C_{2v} symmetry, we also include statistical weights for equivalent exchangeable nuclei for correct transition intensities. Identical to PhCN, there are two sets of equivalent hydrogen atoms ($I_1 = I_2 = \frac{1}{2}$) that give rise to Fermi–Dirac statistics for symmetric (even K) and antisymmetric (odd K) rotational states with a ratio of $10 : 6$ [4].

3.2. Vibrational spectroscopy

The infrared spectrum of PhC_3N is presented in Fig. 3 together with a simulation of the vibrational fundamentals predicted by our anharmonic quantum chemical calculations. At our experimental resolution, the rotational contour of most bands is evident in the spectrum. Because the simulation is in very good agreement with the experiment, numerous assignments can be made with confidence. For ambiguous assignments, two criteria can be invoked: (i) *c*-type bands (B_1 symmetry) exhibit a sharp Q-branch; and (ii) *a*-type bands (A_1) are usually narrower than the others (as can be seen on the simulated spectrum). Out of the 36 active infrared modes of PhC_3N, 14 can be assigned with little or no ambiguity while 9 other bands have tentative assignments at this juncture; the remaining bands are either weak or are predicted in crowded regions of the spectrum (see Table 1 for a detailed list of the proposed assignments). Experimental band centers are taken as the frequency of the Q-branch when one exists (*c*-type bands), equidistant between the *P*- and *R*-branches, or at the maximum of the envelope when no clear contour is visible. Considering *c*-type Q-branches are several wavenumbers wide, an accuracy of ± 2 cm^{-1} can be expected for the band centers with B_1 symmetry. For the others, a conservative value of ± 5 cm^{-1} is proposed.

A few of the assignments proposed in Fig. 3 and Table 1 warrant further discussion. While the assignment of the ν_{26} band (out-of-plane backbone motion) is relatively secure thanks to the presence of a sharp Q-branch, the band appears stronger than expected from our calculations. A possible explanation is that ν_{39} (C≡C—C≡N rocking), predicted roughly at the same frequency as ν_{26}, contributes to the experimental band profile, thus enhancing absorption. In absence of any specific feature arising from ν_{39} on the experimental spectrum, we have chosen to assign this band to the same band center as ν_{26}, at 69 cm^{-1}. Slightly higher in frequency are ν_{25} and ν_{38}, which involve similar nuclear motion as ν_{26} and ν_{39} and are also predicted to lie close in energy (at 192 and 221 cm^{-1}, respectively), which in combination likely yield the feature observed around 200 cm^{-1}. It is not straightforward, however, to unambiguously assign each band center, in part because ν_{25} is the only band of B_1 symmetry with a sizeable transition moment that does not exhibit a sharp Q-branch. Tentative assignments are proposed in Table 1, but their accuracy should be taken with caution as the actual bands centers could lie in a 10 to 20 cm^{-1} window from the proposed assignments. Concerning
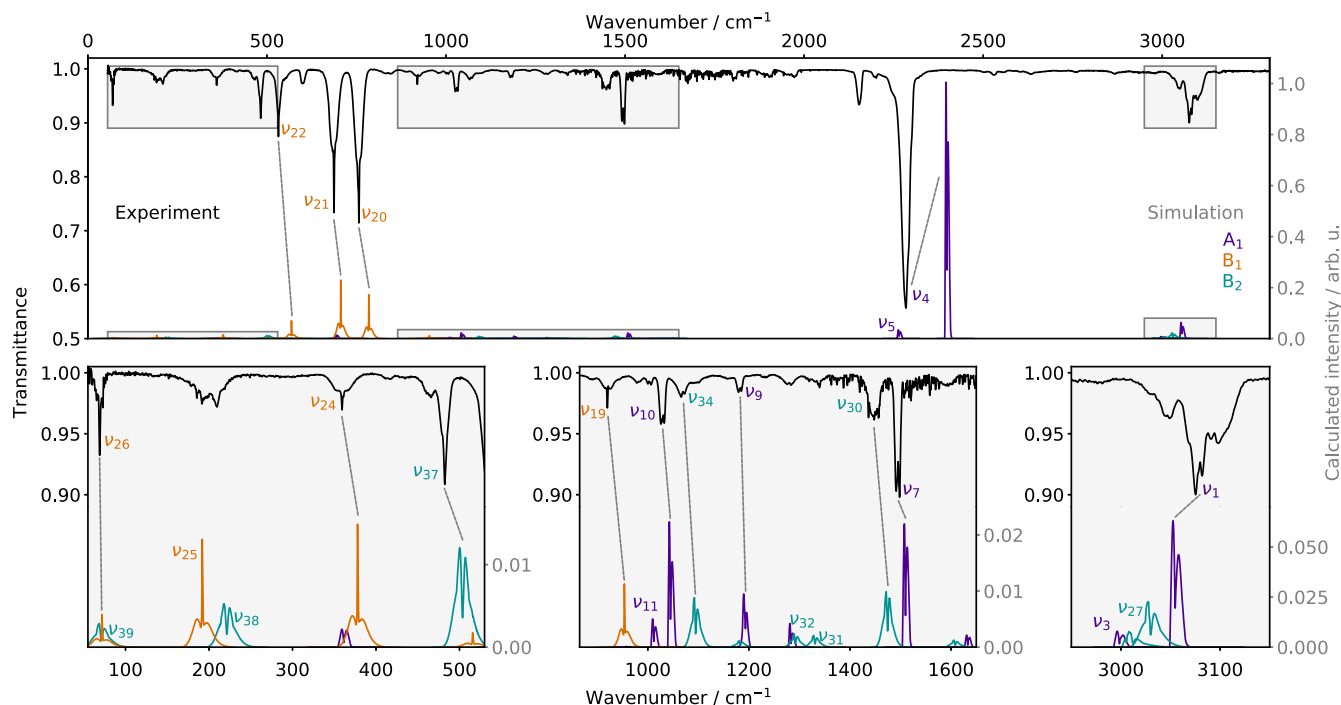
Fig. 3. Experimental (top traces, in black) and simulated (bottom traces, at 300 K, where different colors correspond to different symmetries) vibrational spectrum of PhC_3N. The three bottom panels are expanded portions of the full spectrum, as indicated by gray rectangles. Simulation performed using the PGOPHER software [27] and the results of the anharmonic calculations (band centers, intensities, and rotational constants) and normalized to the strongest IR active mode (v_4). The simulations are inverted relative to the observed spectrum solely for comparison purposes. Secure band assignments are indicated by dash lines; additional labelled bands are those for which an assignment is proposed; simulated bands without any labels remain unassigned.

v_{11} (ring symmetric breathing) and v_5 (C≡C—C≡N stretch)—predicted at 1012 and 2265 cm^{-1}, respectively—two bands lie systematically close to the expected energy, with reasonable band profiles, thus in each case both assignments are reported in Table 1. In the case of v_5, the lowest frequency assignment, *i.e.*, 2154 cm^{-1} appears most likely as the relatively strong intensity of the observed band would indicate a fundamental that could otherwise not be predicted. However the shape of the band lying at 2198 cm^{-1} is closer to that expected for an *a*-type band, assuming that our aforementioned criterion remains valid at these frequencies (*i.e.,* hot bands and combination bands could significantly affect the simplistic fundamentals-only picture).

The most difficult analysis lies in the $\sim 3000 - 3200$ cm^{-1} region, where C—H stretching motions are observed. From previous studies on similar molecules like phenylacetylene [14] and naphthalene [16], it is well-known that this frequency range is plagued by anharmonic resonances which can significantly complicate assignment. For PhC_3N, three modes of A_1 (v_1, v_2, v_3) and two of B_2 (v_{27}, v_{28}) symmetries (Table 1) lie very close in energy (of order of ~10 cm^{-1} for the harmonic frequencies) and can mix strongly, thus qualitatively shifting the fundamental energies and altering band intensities. In such cases, an approximate deperturbation analysis was performed using the generalized VPT2 calculations to identify and treat anharmonic resonances, e.g. those arising from Fermi (so-called "1–2" resonances) and Darling-Dennison ("1–1" interactions in the present case). These resonances are identified based on small differences in the energies of states and a model variational calculation [30]; the former is a zeroth order estimate for resonances, while the latter tests for the magnitude of the coupling [31].

The VPT2 routines in Gaussian treat the problem of state-to-state coupling as effective 2×2 Hamiltonians, where the diagonal elements correspond to the state energies, and the off-diagonal elements represent coupling between the two states. These values

are shown in Table 2, and give rise to significant deviation from the harmonic frequencies and intensities shown in Table 1. Of particular note is the unintuitive complete loss of intensity in v_2 : v_3 is "dark" in the harmonic approximation, and it gains intensity primarily through borrowing intensity from the stronger v_1 and v_2 bands. In a general resonance picture, this interaction shares intensity, and to render a mode completely inactive is extremely rare if not unheard of. Given the VPT2 treatment here is only approximate, our effective deperturbation analysis is likely inadequate to properly treat these bands, and a fully coupled model involving fundamentals, combination bands, and overtones, is required instead.

In light of this preliminary analysis, however, as well as the fact that the ~ 3000 cm^{-1} region is heavily congested, we assume all three A_1 modes are IR active. Measurement under cold conditions—either in a supersonic jet or buffer gas cell—will help future analysis of this molecule by eliminating the possibility of combination bands and overtones, in addition to minimizing lineshape blending from rotational contours. Similarly, selective deuteration might clarify the assignment of some features [14].

3.3. Rotational spectroscopy

Using the ground state rotational and quartic centrifugal distortion constants from the anharmonic calculation, 65 strong lines of the CP-FTMW spectrum were assigned in a straightforward fashion using the PGOPHER software [27] (Fig. 2). The derived values are extremely close to those predicted by the calculation (the weighted frequency difference δ is less than 1% for the rotational constants, see Table 3). This initial set of constants was then used to assign the millimeter-wave data. Loomis-Wood diagrams were produced by means of the LWWa software from Lodyga et al. [32] to aid in the assignment of the high-J transitions. In total,

Table 1

Fundamental vibrational bands (position and intensity) of PhC$_3$N from the quantum chemical calculations performed in this work at the harmonic and anharmonic levels of theory, and proposition of assignments. Modes are numbered following the anharmonic calculations frequency order. Modes energy are in wavenumbers, intensities are in km/mol, δ values are in %. The experimental assignments are split in two categories, the relatively secure ones (column "Assign.") and the tentative ones (column "Prop."); δ values of the latter are reported in italics.

Mode		Harm. Calc.		Anharm. Calc.		Exp.		
ν	Sym.	Energy	Int.	Energy	Int.	Assign.	Prop.	δ[a]
1	A$_1$	3214	6.7	3055	13.5	3078		0.8
2	A$_1$	3226	5.6	3026	0.0		3047	*0.7*
3	A$_1$	3197	0.0	2999	1.7		3047	*1.6*
4	A$_1$	2431	242.3	2399	220.1	2284		−4.8
5	A$_1$	2292	10.7	2265	7.5		2154/2198	*−4.9/−3.0*
6	A$_1$	1675	1.0	1633	0.5			
7	A$_1$	1545	7.7	1510	4.9	1495		−1.0
8	A$_1$	1306	1.6	1284	0.8			
9	A$_1$	1214	2.1	1193	2.0	1182		−0.9
10	A$_1$	1064	4.6	1045	4.5	1029		−1.5
11	A$_1$	1027	1.3	1012	1.0		1004/981	*−0.8/−3.1*
12	A$_1$	981	0.1	960	0.0			
13	A$_1$	706	3.4	693	3.5			
14	A$_1$	371	0.8	362	0.5			
15	A$_2$	1019	0.0	1000	0.0			
16	A$_2$	876	0.0	862	0.0			
17	A$_2$	413	0.0	412	0.0			
18	B$_1$	1042	0.0	1023	0.0			
19	B$_1$	967	2.8	953	2.4	920		−3.5
20	B$_1$	792	38.7	784	32.7	757		−3.4
21	B$_1$	716	36.7	706	42.7	687		−2.6
22	B$_1$	576	13.2	568	12.4	532		−6.3
23	B$_1$	523	0.2	515	0.3			
24	B$_1$	384	2.8	377	2.8	359		−4.9
25	B$_1$	195	2.6	192	2.5		185	*−3.4*
26	B$_1$	74	0.6	71	0.7	69		−3.3
27	B$_2$	3206	1.9	3030	9.5		3095	*2.1*
28	B$_2$	3222	8.4	3012	2.6			
29	B$_2$	1646	0.7	1608	0.5			
30	B$_2$	1493	8.6	1475	4.5	1448		−1.8
31	B$_2$	1364	1.2	1331	0.9		1336	*0.4*
32	B$_2$	1320	1.3	1292	1.0		1280	*−0.9*
33	B$_2$	1193	0.4	1183	0.5			
34	B$_2$	1117	4.4	1094	3.8	1069		−2.3
35	B$_2$	644	0.0	635	0.0			
36	B$_2$	584	0.5	574	0.4			
37	B$_2$	511	5.3	504	5.6	482		−4.3
38	B$_2$	226	2.3	221	2.4		209	*−5.6*
39	B$_2$	71	1.1	71	1.2		69	*−2.7*

[a] $\delta = $ (Exp. − Anharm.Calc.)/Anharm.Calc. $\times$ 100.

Table 2

Strong anharmonic resonances and their corresponding off-diagonal matrix elements for bands in the ~ 3100 − 3200 cm^{-1} region. Darling-Dennison (DDR) and Fermi (FR) resonances are indicated; in this table, the former corresponds to 1 − 1 type DDR, referring to the number of quanta for states involved.

State 1	State 2	Type	Coupling
$\nu_1 = 1$	$\nu_3 = 1$	DD	−6.6
$\nu_2 = 1$	$\nu_3 = 1$	DD	14.5
$\nu_3 = 1$	$\nu_6 = 1 + \nu_7 = 1$	FR	−23.2
$\nu_3 = 1$	$\nu_{29} = 1 + \nu_{30} = 1$	FR	−29.3
$\nu_{27} = 1$	$\nu_{28} = 1$	DD	9.4

6151 a-type transitions (3780 different frequencies as a result of unresolved asymmetric splitting) of PhC$_3$N in its ground vibrational state were assigned in the millimeter-wave spectrum, with values of J'' up to 199 and K_a'' up to 42.

The SPFIT/SPCAT suite of programs [33] using the Watson S-reduced Hamiltonian in the I^r representation was used to determine best-fit spectroscopic constants. All transitions were weighted accorded to their expected experimental accuracy, *i.e.*,

2 kHz and 25 kHz for the CE-FTMW and CP-FTMW transitions, respectively, and 50 kHz for the millimeter-wave transitions. To reproduce the data to their experimental accuracy, inclusion of several sextic and octic centrifugal distortion constants was required. Finally, the CE-FTMW transitions—the only ones for which the nuclear quadrupole splitting was resolved—were added to the fit to determine the χ(N) terms. All 57 hyperfine components were reproduced to the measurement uncertainty by adjusting only χ_{aa}(N) and χ_{bb}(N). Both parameters are close to those expected from calculation (to within about 15%, Table 3). When a transition was observed by both CP-FTMW and CE-FTMW spectroscopy, only the latter was retained in the fit, owing to the higher frequency accuracy of the cavity instrument. The rotational constants derived from a fit to all of the assigned rotational transitions are reported in Table 3. The final 49 kHz RMS value of the fit, corresponding to a reduced standard deviation $\sigma = 1.00$, indicates that our present model adequately reproduces the ground state rotational spectrum of PhC$_3$N.

Fig. 4 shows a portion of the millimeter-wave spectrum in comparison with a simulation of PhC$_3$N in its vibrational ground

Table 3

Spectroscopic constants (rotational, centrifugal distorsion, and nuclear quadrupole constants) of PhC_3N in its vibrational ground state (in MHz) and relevant fit parameters. Numbers in parenthesis are 1σ uncertainties expressed in the unit of the last digit. Parameters in brackets were kept fixed to the calculated values.

Constant	Calc.[a]	Exp.	δ[b]
A_0	5656.9	5659.722 (15)	0.05
B_0	567.0	569.582206 (39)	0.46
C_0	515.4	517.404488 (37)	0.39
$D_J \times 10^6$	3.6	3.85110 (77)	7.0
$D_{JK} \times 10^3$	0.78	0.827177 (85)	6.1
$D_K \times 10^3$	0.42	0.400 (68)	−4.8
$d_1 \times 10^6$	−0.50	−0.55191 (24)	10
$d_2 \times 10^6$	−0.52	−0.57101 (79)	9.8
$H_J \times 10^{12}$		−0.957 (11)	
$H_{JK} \times 10^9$		0.7916 (18)	
$H_{KJ} \times 10^6$		−0.03051 (10)	
$h_2 \times 10^{12}$		0.575 (15)	
$h_3 \times 10^{12}$		0.10329 (55)	
$L_{JJK} \times 10^{15}$		−1.295 (20)	
$L_{JK} \times 10^{12}$		0.06954 (86)	
$L_{KKJ} \times 10^{12}$		−3.512 (36)	
χ_{aa}	−4.96	−4.219 (77)	−15
χ_{bb}	2.39	2.114 (68)	−12
χ_{cc}	2.57	2.143[c]	−17
N[d]		6256/3877/57	
$J''_{max}, K''_{a\,max}$		199, 42	
rms/kHz		0.049	
σ[e]		1.00	

[a] ωB97XD/cc-pVQZ level of theory, Bayesian corrected for A, B, and C, and anharmonic values for the centrifugal distortion constants, and equilibrium values for the hyperfine constants.

[b] $\delta = (B_{exp.} - B_{calc.})/B_{calc.} \times 100$ (in %).

[c] Derived value.

[d] Total number of lines in the fit/ Number of different frequencies/ Number of lines with resolved nuclear quadrupole structure.

[e] Reduced standard deviation, unitless.

state using the experimentally determined best-fit parameters from Table 3. As illustrated in this figure, many lines remain unassigned, but most of these likely arise from vibrational satellites, for which no attempt at assigning was made in the present study. Although longer integration times would allow a more in-depth analysis of these satellites, the spectrum is already fairly dense, implying that we may be close to the confusion limit. Indeed, the 2 μbar pressure used in this study, although quite low, was actually a compromise between reasonable signal-to-noise ratio and pressure broadening. Even at this pressure many lines are broader then expected from the effects of pressure broadening alone, and consequently may in fact be a spectral superposition of several transitions.

Regarding hyperfine splitting, its magnitude rapidly collapses with increasing J, as expected from this type of interaction. No splitting is observed in the CP-FTMW nor in millimeter-wave measurements, and in the cavity experiments it is marginally resolved above $J'' \approx 11$ (~ 12 GHz). Even at the lowest-J transitions measured here ($J'' = 5, \sim 6$ GHz), the splitting due to hyperfine and Doppler effects are comparable (Fig. 5). The experimentally derived value of $\chi_{aa}(N)$ [−4.219 (77) MHz; Table 3] is very similar to that reported for PhCN [−4.23738 (36) MHz [9]], and the relative magnitudes are in agreement with the theoretical values of $\chi_{aa}(N)$ calculated at the ωB97X-D/cc-pVQZ level of theory for PhC_3N (−4.959 MHz) and PhCN (−4.962 MHz). The small changes in χ(N) are an indication that the local electronic structure of the nitrogen atom is relatively insensitive to the distance from the aromatic ring. Equivalently, this finding implies that electron delocalization through ring conjugation is very poorly coupled to the chain regardless of length. Similar behavior is seen for cyano-polyyne chains, where the value of eQq equivalent to $\chi_{aa}(N)$ (around −4.1 MHz) is relatively invariant with the length of the chain as well [34].
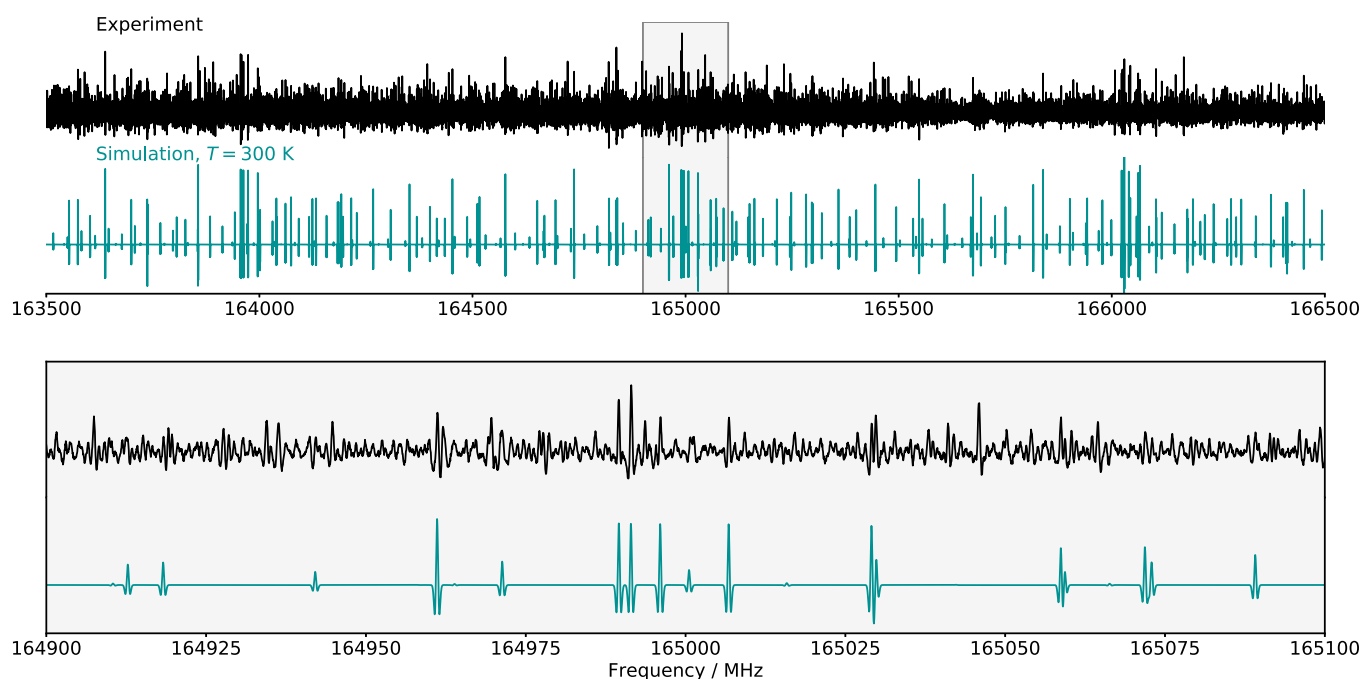

Fig. 4. Portions of the millimeter-wave spectrum of PhC_3N in comparison with a simulation of the pure rotational transitions in the ground vibrational state using the best-fit set of spectroscopic constants (Table 3). The simulation has been performed using the PGOPHER software and the resulting trace was then post-processed with a second derivative to allow a more straightforward comparison with the experimental spectrum. The line density in the experimental trace is far greater than our simulation, very likely because of lines from vibrational satellites.
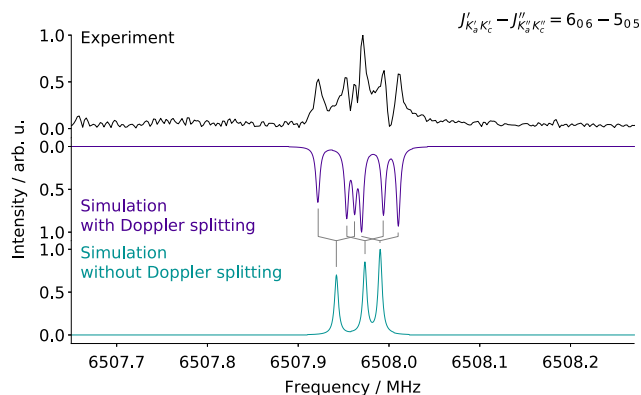
Fig. 5. Example of a transition showing resolved hyperfine structure on the CE-FTMW spectrum, and comparison with 10 K simulations using the final set of spectroscopic parameters, with and without taking into account the Doppler splitting (simulations performed using the PGOPHER software, assuming a Lorentzian lineshape). As before, the simulation with Doppler splitting is inverted relative to the observed spectrum solely for comparison purposes.

Fig. 6. Calculated rotational spectrum of PhC$_3$N at 10 K (purple), 100 K (blue), and 300 K (orange). For the purposes of display, these relative intensities for the 100 K plot have increased by a factor of 5, while for the 300 K plot, the increase is 10.

3.4. Astronomical considerations

Detection of molecules in space by radio astronomy is heavily dependent on the magnitude of their permanent dipole moment. In comparison with PhCN, our theoretical predictions suggest PhC$_3$N is substantially more polar (5.9 D vs. of 4.5 D, where the former value has statistical uncertainty of ± 0.25 D based on our prior benchmarking at the ωB97X-D/cc-pVQZ level of theory [35]). Currently, PhCN is theorized to form in cold, dark clouds via a barrierless reaction between C$_6$H$_6$ and CN radical [4,36]. We thus speculate that PhC$_3$N could be formed via C$_2$ insertion to PhCN or through an analogous C≡N addition reaction between CN radical and phenylacetylene (PhC$_2$H), or C$_3$N and C$_6$H$_6$. If the latter mode is operative, then the abundance ratio of PhCN/PhC$_3$N will be dependent on CN/C$_3$N, assuming similar reaction cross-sections. The CN + PhC$_2$H process has been studied in crossed-beam experiments by Bennett et al. [11], where the authors identify PhC$_3$N as a potential reaction product, albeit not definitively so due to the lack of isomer specificity and at collision energies well in excess of interstellar cloud conditions ($\sim$ 30 kJ/mol). This finding suggests other isomers, namely *ortho, meta, para*-CEB, might plausibly be formed from this reaction. While we have not attempted to experimentally characterize these species, estimates of their spectroscopic parameters are provided here. By scaling the experimental parameters for PhC$_3$N (Table 3) to correct for vibrational and electronic effects (Table S6 in the Supporting Information), in conjunction to Bayesian uncertainties obtained from benchmarking [35], reliable constraints of these constants should aid future experimental searches for these species.

In terms of astronomical detection, although the hyperfine structure does not take a large part the present rotational analysis, this splitting is partially resolved with cavity measurements up to 16 GHz. In cold, dark clouds such as TMC-1 where the linewidths are comparable to those measured with our CE-FTMW spectrometer, it is thus necessary to consider hyperfine splitting, as recent work on PhCN [4] demonstrates. This is particularly true for a relatively heavy molecule like PhC$_3$N whose strongest lines should lie at centimeter-wavelengths at low temperatures (Fig. 6): at 10 K, the strongest features correspond to $J'' = 21$ around 23 GHz, while at 6 K —a typical temperature for molecules in TMC-1— the strongest features are near 15 GHz ($J'' = 14$). Thus, the X/K$_u$ (8–12/12–18 GHz) bands appear to be the most promising to detect PhC$_3$N in TMC–1. In sources with somewhat warmer temperatures, the intensity of individual transitions is significantly decreased due
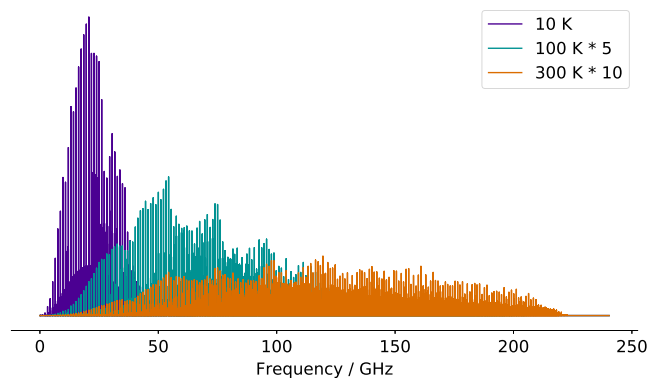
to the larger partition function, and the peak intensity, although relatively flat, falls in the W (75–110 GHz) and N (100–200 GHz) bands.

Detection of multiple isomers is also a powerful tool for constraining physical and chemical conditions in astrophysical environments. To assist in this process, we have calculated the relative energy of the aforementioned *ortho, meta,* and *para*-CEB isomers, along with the isocyanide isomer, PhCCNC. As shown in Fig. 7, apart from the isocyanide isomer, placement of the acetylenic unit on different parts of the ring produces isomers with comparable stability to PhC$_3$N, *i.e.*, they are effectively degenerate at the level of uncertainty afforded by G3//B3LYP (± 4 kJ/mol). As such, a determination of their relative abundances would provide a sensitive test of thermodynamics vs. kinetics in molecule formation. To aid further laboratory and hopefully astronomical efforts, Table S6, in addition to providing estimates of rotational constants, also reports calculated dipole moments at the ωB97X-D/cc-pVQZ level of theory using two methods of empirical scaling to correct for vibrational effects and deficiencies in the electronic structure method. We note that the Bayesian scaling factors obtained in
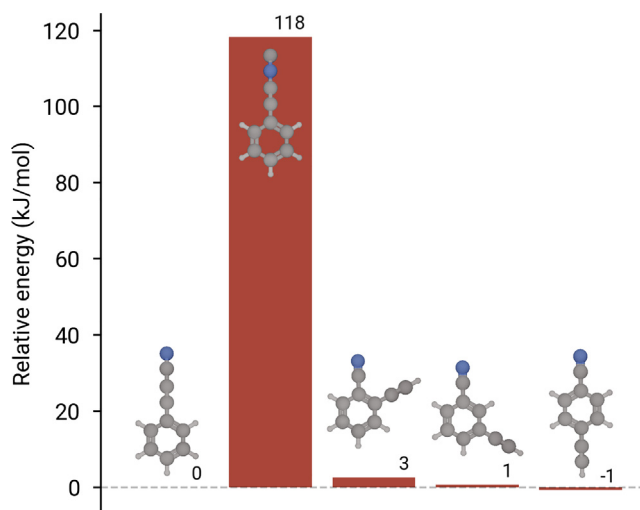

Fig. 7. 0 K energetics of isomers of interest calculated at the G3//B3LYP level of theory, relative to PhC$_3$N. Energies to the nearest kJ/mol are annotated above each bar.

Ref. [35] applied to PhC$_3$N —where we now have accurately determined parameters— exceed the performance of the purely theoretical VPT2 corrections, and bring the theoretical predictions within a few MHz of the experimentally measured ones (see also Fig. S1). We expect a similar degree of precision and uncertainty for other isomers.

4. Conclusion

Using a combination of gas-phase measurements and quantum chemical calculations, the fundamental vibrational frequencies of most of the strongest IR-active fundamentals of PhC$_3$N and over 6000 pure rotational transitions in its ground state between 6.5 and 220 GHz have been measured. The assignment of spectra in different regions was guided by theoretical predictions: in the infrared, anharmonic calculations helped to assign most bands, with the exception of the most congested and perturbed region around 3000 cm^{-1}; in the radio domain, estimates of centrifugal distortion and hyperfine terms proved useful. Comparisons with PhCN suggest that the local electronic structure of the terminal nitrogen —as probed through its quadrupole moment $\chi_{aa}(N)$— is relatively unaffected by chain lengthening, indicating a similar electric field gradient for nitrogen in both PhCN and PhC$_3$N. In addition, we provide accurate and reliable predictions of the thermochemistry and spectroscopic parameters for several isomers of PhC$_3$N, which should prove useful in guiding future laboratory experiments. These isomers include the isocyanide isomer of PhC$_3$-N and the three cyanoethynylbenzenes alluded to in previous work [11]; their discovery along with PhC$_3$N in the ISM would provide sensitive measurements of local chemical and physical interstellar environments.

With highly precise measurements of the rest frequencies and corresponding spectroscopic constants, a search for PhC$_3$N can now be undertaken with considerable confidence in the ISM. The large permanent dipole moment (predicted to be 5.9 D), in addition to its chemical and structural similarity to astronomical PhCN makes PhC$_3$N an excellent candidate for detection towards cold, dark molecular clouds such as TMC-1. Hyperfine-resolved measurements are expected to be highly relevant in a potential discovery, given that at low temperatures the strongest transitions lie in the X/K$_u$ bands where the splitting is comparable to the source linewidth.

Declaration of Competing Interest

The authors declare that they have no known competing financial interests or personal relationships that could have appeared to influence the work reported in this paper.

Acknowledgements

Appendix A. Supplementary material

Supplementary data associated with this article can be found, in the online version, at https://doi.org/10.1016/j.jms.2021.111425.

References

[1] M. Frenklach, E.D. Feigelson, Formation of polycyclic aromatic hydrocarbons in circumstellar envelopes, Astrophys. J. 341 (1989) 372.

[2] T.P. Snow, A.N. Witt, The interstellar carbon budget and the role of carbon in dust and large molecules, Science 270 (1995) 1455–1460.

[3] A. Tielens, Interstellar polycyclic aromatic hydrocarbon molecules, Ann. Rev. Astron. Astrophys. 46 (2008) 289–337.

[4] B.A. McGuire, A.M. Burkhardt, S. Kalenskii, C.N. Shingledecker, A.J. Remijan, E. Herbst, M.C. McCarthy, Detection of the aromatic molecule benzonitrile (c-C6H5CN) in the interstellar medium, Science 359 (2018) 202–205.

[5] D. McNaughton, M.K. Jahn, M.J. Travers, D. Wachsmuth, P.D. Godfrey, J.-U. Grabow, Laboratory rotational spectroscopy of cyano substituted polycyclic aromatic hydrocarbons, Mon. Not. R. Astron. Soc. 476 (2018) 5268–5273.

[6] M.C. McCarthy, K.L.K. Lee, R.A. Loomis, A.M. Burkhardt, C.N. Shingledecker, S.B. Charnley, M.A. Cordiner, E. Herbst, S. Kalenskii, E.R. Willis, C. Xue, A.J. Remijan, B.A. McGuire, Interstellar detection of the highly polar five-membered ring cyanocyclopentadiene, Nature Astronomy 5 (2021) 176–180.

[7] T. Gautier, N. Carrasco, A. Buch, C. Szopa, E. Sciamma-O'Brien, G. Cernogora, Nitrile gas chemistry in Titan atmosphere, Icarus 213 (2011) 625.

[8] R. Loomis, et al., The third time's a charm? A rigorous investigation of spectral line stacking techniques and application to the detection of HC11N, submitted (2020).

[9] K. Wohlfart, M. Schnell, J.-U. Grabow, J. Küpper, Precise dipole moment and quadrupole coupling constants of benzonitrile, J. Mol. Spectrosc. 247 (2008) 119–121.

[10] B. Bak, D. Christensen, W.B. Dixon, L. Hansen-Nygaard, J. Rastrup-Andersen, Benzene ring distortion by one substituent. microwave determination of the complete structure of benzonitrile, J. Chem. Phys. 37 (1962) 2027–2031. Publisher: American Institute of Physics.

[11] C.J. Bennett, S.B. Morales, S.D.L. Picard, A. Canosa, I.R. Sims, Y.H. Shih, A.H.H. Chang, X. Gu, F. Zhang, R.I. Kaiser, A chemical dynamics, kinetics, and theoretical study on the reaction of the cyano radical (CN; X$^2\Sigma^+$) with phenylacetylene (C6H5CCH; X^{1}A$_1$), Phys. Chem. Chem. Phys. 12 (2010) 8737–8749.

[12] K.M. Jawad, T.S. Zwier, L.V. Slipchenko, C.I. Viquez Rojas, The exotic excited state behavior of 3-phenyl-2-propyenitrile, http://hdl.handle.net/2142/97063, 2017. International Symposium on Molecular Spectroscopy.

[13] C.I. Viquez Rojas, L.V. Slipchenko, T.S. Zwier, K.M. Jawad, Computational modeling of electronic spectroscopy of 3-phenyl-2-propyenitrile, http://hdl.handle.net/2142/97102, 2017. International Symposium on Molecular Spectroscopy.

[14] G. King, S. So, Ethynylbenzene; The vibrational spectra of some deuterated isomers, J. Mol. Spectrosc. 36 (1970) 468–487. ZSCC: 0000063.

[15] C.-H. Chang, G. Lopez, T.J. Sears, P.M. Johnson, Vibronic analysis of the S$_1$ -S$_0$ transition of phenylacetylene using photoelectron imaging and spectral intensities derived from electronic structure calculations, J. Phys. Chem. A 114 (2010) 8262–8270. ZSCC: NoCitationData[s0].

[16] O. Pirali, M. Vervloet, G. Mulas, G. Malloci, C. Joblin, High-resolution infrared absorption spectroscopy of thermally excited naphthalene. Measurements and calculations of anharmonic parameters and vibrational interactions, PCCP 11 (2009) 3443. ZSCC: 0000046.

[17] O. Pirali, Z. Kisiel, M. Goubet, S. Gruet, M.A. Martin-Drumel, A. Cuisset, F. Hindle, G. Mouret, Rotation-vibration interactions in the spectra of polycyclic aromatic hydrocarbons: Quinoline as a test-case species, J. Chem. Phys. 142 (2015) 104310. Publisher: American Institute of Physics.

[18] Z. Kisiel, A. Krasnicki, The millimetre-wave rotational spectrum of phenylacetylene, J. Mol. Spectrosc. 262 (2010) 82–88.

[19] M.A. Zdanovskaia, B.J. Esselman, H.S. Lau, D.M. Bates, R.C. Woods, R.J. McMahon, Z. Kisiel, The 103–360 GHz rotational spectrum of benzonitrile, the first interstellar benzene derivative detected by radioastronomy, J. Mol. Spectrosc. 351 (2018) 39–48.

[20] M.J. Frisch, G.W. Trucks, H.B. Schlegel, G.E. Scuseria, M.A. Robb, J.R. Cheeseman, G. Scalmani, V. Barone, G.A. Petersson, H. Nakatsuji, X. Li, M. Caricato, A.V. Marenich, J. Bloino, B.G. Janesko, R. Gomperts, B. Mennucci, H.P. Hratchian, J.V. Ortiz, A.F. Izmaylov, J.L. Sonnenberg, D. Williams-Young, F. Ding, F. Lipparini, F. Egidi, J. Goings, B. Peng, A. Petrone, T. Henderson, D. Ranasinghe, V.G. Zakrzewski, J. Gao, N. Rega, G. Zheng, W. Liang, M. Hada, M. Ehara, K. Toyota, R. Fukuda, J. Hasegawa, M. Ishida, T. Nakajima, Y. Honda, O. Kitao, H. Nakai, T. Vreven, K. Throssell, J.A. Montgomery, Jr., J.E. Peralta, F. Ogliaro, M.J. Bearpark, J.J. Heyd, E.N. Brothers, K.N. Kudin, V.N. Staroverov, T.A. Keith, R. Kobayashi, J. Normand, K. Raghavachari, A.P. Rendell, J.C. Burant, S.S. Iyengar, J. Tomasi, M. Cossi, J.M. Millam, M. Klene, C. Adamo, R. Cammi, J.W. Ochterski, R. L. Martin, K. Morokuma, O. Farkas, J.B. Foresman, D.J. Fox, Gaussian 16 Revision A.01, 2016.

[21] A.G. Baboul, L.A. Curtiss, P.C. Redfern, K. Raghavachari, Gaussian-3 theory using density functional geometries and zero-point energies, J. Chem. Phys. 110 (1999) 7650–7657.

[22] J.M. Simmie, K.P. Somers, Benchmarking compound methods (CBS-QB3, CBS-APNO, G3, G4, W1BD) against the active thermochemical tables: a litmus test for cost-effective molecular formation enthalpies, J. Phys. Chem. A 119 (2015) 7235–7246.

[23] J.-B. Brubach, L. Manceron, M. Rouzières, O. Pirali, D. Balcon, F. Kwabia-Tchana, V. Boudon, M. Tudorie, T. Huet, A. Cuisset, P. Roy, in: WIRMS 2009, volume 1214 of AIP Conference Proceedings, 2010, pp. 81–84.

[24] M. Faye, M. Bordessoule, B. Kanouté, J.-B. Brubach, P. Roy, L. Manceron, Improved mid infrared detector for high spectral or spatial resolution and synchrotron radiation use, Rev. Sci. Instrum. 87 (2016) 063119.

[25] O. Pirali, M. Goubet, T.R. Huet, R. Georges, P. Soulard, P. Asselin, J. Courbe, P. Roy, M. Vervloet, The far infrared spectrum of naphthalene characterized by high resolution synchrotron FTIR spectroscopy and anharmonic DFT calculations, PCCP 15 (2013) 10141–10150.

[26] K.N. Crabtree, M.-A. Martin-Drumel, G.G. Brown, S.A. Gaster, T.M. Hall, M.C. McCarthy, Microwave spectral taxonomy: A semi-automated combination of chirped-pulse and cavity fourier-transform microwave spectroscopy, J. Chem. Phys. 144 (2016) 124201.

[27] C.M. Western, PGOPHER: a program for simulating rotational, vibrational and electronic spectra, J. Quant. Spectrosc. Radiat. Transfer 186 (2017) 221–242.

[28] M.C. McCarthy, K.L.K. Lee, P.B. Carroll, J.P. Porterfield, B. Changala, J.H. Thorpe, J.F. Stanton, Exhaustive product analysis of three benzene discharges by microwave spectroscopy, J. Phys. Chem. A (2020).

[29] O. Pirali, M. Goubet, V. Boudon, L. D'Accolti, C. Fusco, C. Annese, Characterization of isolated 1-aza-adamantan-4-one (C9H13NO) from microwave, millimeter-wave and infrared spectroscopy supported by electronic structure calculations, J. Mol. Spectrosc. 338 (2017) 6–14.

[30] J.M.L. Martin, T.J. Lee, P.R. Taylor, J. François, The anharmonic force field of ethylene, C_2h_4, by means of accurate ab initio calculations, J. Chem. Phys. 103 (1995) 2589–2602. ZSCC: NoCitationData[s0]..

[31] J. Bloino, M. Biczysko, V. Barone, Anharmonic effects on vibrational spectra intensities: infrared, Raman, vibrational circular dichroism, and Raman optical activity, J. Phys. Chem. A 119 (2015) 11862–11874.

[32] W. Lodyga, M. Kreglewski, P. Pracna, Urban, Advanced graphical software for assignments of transitions in rovibrational spectra, J. Mol. Spectrosc. 243 (2007) 182–188. PRAHA2006, The 19th International Conference on High Resolution Molecular Spectroscopy..

[33] H.M. Pickett, The fitting and prediction of vibration-rotation spectra with spin interactions, J. Mol. Spectrosc. 148 (1991) 371–377.

[34] M.C. McCarthy, W. Chen, M.J. Travers, P. Thaddeus, Microwave spectra of 11 polyyne carbon chains, Astrophys. J. Suppl. Series 129 (2000) 611.

[35] K.L.K. Lee, M. McCarthy, Bayesian Analysis of Theoretical Rotational Constants from Low-Cost Electronic Structure Methods, J. Phys. Chem. A 5 (2020) 898–910.

[36] K.L.K. Lee, B.A. McGuire, M.C. McCarthy, Gas-phase synthetic pathways to benzene and benzonitrile: a combined microwave and thermochemical investigation, PCCP 21 (2019) 2946–2956.